

Metallicities in long GRB host galaxies at $z < 0.5$ calculated by the detailed modelling of optical and infrared line ratios

M. Contini

School of Physics and Astronomy, Tel Aviv University, Tel Aviv 69978, Israel

13 June 2021

ABSTRACT

We revisited the line spectra emitted from long GRB (LGRB) host galaxies at $z \leq 0.5$ in order to calculate by the detailed modelling of the line ratios, the physical conditions and relative abundances in LGRB hosts in this redshift range. We have found lower metallicities than in LGRB hosts at higher z . New results about metallicities and physical conditions in the different regions throughout the LGRB 980425 host at $z=0.0085$ are presented. In particular, we have found that the effective starburst temperature in the supernova (SN) region is the highest throughout the host galaxy. The low ionization parameter reveals that the radiation source is far or somehow prevented from reaching the emitting gas in the SN region. The models constrained by a few oxygen, nitrogen and sulphur line ratios to $H\beta$ in LGRB 980425 host satisfactorily reproduce the $HeII/H\beta$ and $[ArIII]/H\beta$ line ratios. The modelling of the observed $[SIV]10.51\mu m / [SIII]18.71\mu m$ and $[NeIII]10.6\mu m / [NeII]12.81\mu m$ line ratios from LGRB 031203 host galaxy at $z=0.105$ shows that the mid-IR lines are emitted from geometrically thin shock dominated filaments which are not reached by the photoionizing flux, while the optical lines are emitted from the radiation dominated outflowing clouds.

Key words: radiation mechanisms: general — shock waves — ISM: abundances — galaxies: GRB — galaxies: high redshift

1 INTRODUCTION

Long duration γ -ray bursts (LGRB) derive from the death of very massive star (e.g. Paczynski 1998), they are flashes of cosmic high energy (~ 1 keV – 10 GeV) photons (Fishman & Meegan 1995) and explode in star forming galaxies. LGRB and their afterglows are associated with broad lined SN Ic (e.g. Hjorth et al 2003, Stanek et al 2003). The analysis of LGRB host galaxy emission lines provides information about star-forming galaxies at high z (e.g. Krühler et al 2015, Blanchard et al 2015 and references therein). The fluxes of significant oxygen lines, a few nitrogen lines as well as $H\alpha$ and $H\beta$ are available from the surveys at redshifts $z \leq 3$. A few lines appear in the literature at higher z . The strongest lines in the optical range are $[OII]3727+3729$ (hereafter $[OII]3727+$), $[OIII]5007+4959$ (hereafter $[OIII]5007+$) and $[NII]6584$ together with $H\beta$ and $H\alpha$. The $[OIII]4363$ line, which plays a dominant role in the modelling process, is weak and not always available. Some spectra contain also $[NeIII]3869$, $[SII]6717$, $[SII]6731$ and seldom He, Fe and Ar lines (e.g. Hammer et al 2006). The interpretation of the spectra leads to more or less converging theories about the distribution on z of star formation rates, ages, star masses

and temperatures. The most interesting parameters are related to metallicities, such as the O/H relative abundances, followed by the N/H one. Metallicity is one of the main parameters which affects the evolution of massive stars as well as their explosive deaths (Vergani et al 2011, Piranomonte et al 2015, Sollerman et al 2005, Woosley 1993, etc). Niino et al (2016) claim that the relation between metallicity and LGRB occurrence rate is not understood quantitatively because, even when the redshifts of the host galaxies are well known, the host galaxy is "not studied in detail". Such a crucial issue, which yields many consequences in a large z range deserves a more precise analysis.

In a previous paper (Contini 2016) we presented new results calculated by the detailed modelling of LGRB line ratios and we compared them with those obtained by different investigations, in particular for the element abundances in GRB host galaxies at relatively high redshifts. The emission line spectra emitted from LGRB host galaxies on a large z range were collected from the surveys of Krühler et al, Savaglio et al (2009), Sollerman et al (2005), Castro-Tirado et al (2001), Graham & Fruchter (2013), Levesque et al (2010), Vergani et al (2011), Piranomonte et al (2015), the

LGRB line and continuum spectra with Wolf-Rayet (WR) features from the Han et al (2010) survey. In particular, the GRB 980425 host spectrum (Sollerman et al 2005) was selected because the survey refers to relatively low redshift galaxies ($z < 0.2$) that host GRB. Sollerman et al claim that they are star-forming galaxies with luminosities $L < L_{\odot}$ and relatively low metallicity. The spectra include the He I 5876 line which is also significant in SN Type 1c hosts relatively to WR stars.

Contini (2016, fig. 6 top diagram) shows the results of O/H and N/H calculated in each of the LGRB hosts by the detailed modelling of the spectra. O/H is close to solar in most objects. We will conventionally define "solar" relative abundances $(O/H)_{\odot} = 6.6 - 6.7 \times 10^{-4}$ and $(N/H)_{\odot} = 9. \times 10^{-5}$ (Allen 1976, Grevesse & Sauval 1998) that were found suitable to local galaxy nebulae. Moreover, these values are included between those of Anders & Grevesse (1989) (8.5×10^{-4} and 1.12×10^{-4} , respectively) and Asplund et al (2009) (4.9×10^{-4} and 6.76×10^{-5} , respectively). Regarding nitrogen, we note a large distribution of N/H abundance ratios from solar to lower than solar by a factor > 10 in GRB hosts. Subsolar N/H indicates external gas acquisition through galaxy merging processes. Some observed LGRB hosts, however, show high metallicity. Krüler et al (and references therein) point out that "several metal rich GRB were discovered". Graham et al (2015) recently confirmed that high metallicities can be found in LGRB. The near solar O/H relative abundances calculated from the observed line ratios by Contini (2016) in LGRB hosts exceed the O/H values generally obtained by other modelling methods. In particular at high z , lower than solar O/H in the host gas (e.g. Krühler et al 2015) were predicted by modelling the $[OIII]/H\beta$ and $[OII]/H\beta$ line ratios using the strong-line methods (see Sect. 2). These results are generally obtained by the author majority. This issue (see Contini 2014 and references therein) will be explained in the following section.

The number of LGRB galaxy host spectra at relatively low z investigated by Contini (2016) was insufficiently small. In this paper we try to fill this gap, although by a relatively small number of objects, by modelling in detail the LGRB host spectra presented by Niino et al (2016) at $z \leq 0.41$. They explain that the sample number at these redshifts cannot be large because the cosmic LGRB rate density is low. On the other hand, the faint galaxies can be investigated without very deep observations and the host galaxy spectroscopy can give information even when GRB afterglows are not bright enough. In addition, low z GRB host galaxies give a hint about the host characteristics in an epoch close to that of local galaxies, connecting low with high z objects. We will investigate this correlation.

The spectral lines of some galaxies in the Niino et al sample were reported by various observers. They may contain different information in each sample context, therefore we refer to each survey as presented by the observers. For galaxy GRB 980425 host Niino et al refer to the average spectrum presented by Christensen et al (2008), who report for this object at $z=0.0085$ a rich collection of spectra in different locations within the host. We have the rare occasion to calculate the distribution of the physical quantities throughout a galaxy at redshifts higher than local by modelling each of the observed spectra. Moreover, previous spectra presented by Hammer et al (2006) for the GRB 980425

SN, WR star and the "4" regions show many lines which can definitively constrain the models and confirm the presence of the WR stars.

The strongest lines observed in recent years from galaxies at relatively high z are in the optical range. Observations in the infrared (IR) are now available e.g. from Michalowski et al (2016) and Watson et al (2016) showing strong $[CII]158\mu m$, $[OI]63\mu m$ in the far-IR (FIR) and $[SIV]10.51\mu m$, $[SIII]18.71\mu m$, $[NeIII]15.56\mu m$, $[NeII]12.81\mu m$, etc. lines in the mid-IR, respectively. In this paper we will investigate whether the optical lines and the mid-IR and FIR lines from the GRB 0301203 host galaxy are emitted from clouds of gas in similar physical conditions.

We use for the calculation of the line ratios the code SUMA which simulates an emitting gaseous cloud within a galaxy hosting an AGN or a starburst, heated and ionized by the coupled effect of the primary and secondary photoionization fluxes and shocks. Shocks throughout the host galaxies are the product of star explosions and of cloud collisions by e.g. galaxy merging (Contini 2016 and references therein). The "detailed modelling" method is briefly explained and compared with the strong-line methods in Sect. 2. The analysis of Niino et al observed line spectra is presented in Sect. 3 and those of Christensen et al and Hammer et al relatively to the LGRB 980425 host galaxy are investigated in Sect. 4. The optical and IR emission lines observed from LGRB 031203 host are discussed in Sect. 5. Concluding remarks follow in Sect. 6.

2 DETAILED MODELLING OF THE LINE SPECTRA

2.1 Comparison of modelling methods

To calculate the O/H abundance ratio from the observations, "direct methods" (see e.g. Modjaz et al 2008) are generally adopted. They date back to the early '70ties when active galaxy line spectra started to appear (see Seaton 1975, Pagel et al 1992). Later, they were updated. Determination of the O/H relative abundance from the oxygen line ratios to $H\beta$ by current strong-line methods focus on $[OIII]/H\beta$ and $[OII]/H\beta$. The line fluxes depend mostly on the fractional abundance of the ions and on the relative abundance of the elements. In particular, for intermediate ionization- level lines such as $[OII]$ and $[OIII]$, the fractional abundance of the relative ions are high in the radiation dominated zone of the cloud, while strong shocks are necessary to obtain strong lines from high ionization-levels (see, e.g. Sect. 5) and recombined element lines. By detailed modelling, the line fluxes are integrated throughout the recombination region where a large zone of gas is characterized by $T_e < 10^4$ K (see Sect. 5). O^+/O and O^{2+}/O fractional abundances peak at different temperatures. In the cool gas region both are relatively low. Therefore, to reproduce high $[OII]/H\beta$ and $[OIII]/H\beta$ line ratios, relatively high O/H are invoked. By the strong-line models, a single temperature of 10^4 K is generally adopted corresponding to high O^+/O and O^{2+}/O fractional abundances, so relatively low O/H are suitable to fit the observed line ratios. It was explained by Contini (2014) that the metallicities in terms of O/H and N/H obtained by the strong-line methods are

Table 1. Modelling [OII]3727+, [OIII]5007+, $H\alpha$ and [NII]6583 line ratios to $H\beta$ from Niino et al (2016) LGRB host galaxy spectra

	z	[OII]/ $H\beta$	[OIII]/ $H\beta$	$H\alpha$ / $H\beta$	[NII]/ $H\beta$	V_s km s^{-1}	n_0 cm^{-3}	D 10^{18}cm	O/H 10^{-4}	N/H 10^{-4}	T_* 10^4K	U -	$H\beta$ 1
980425 ²	0.0085	5.39	3.86	4.02	0.44	-	-	-	-	-	-	-	-
mN1a	-	5.65	3.86	2.97	0.42	150	80	0.4	5.	0.17	9.	0.0066	0.0041
980425 ³ _c	0.0085	7.09	3.73	3.00	0.32	-	-	-	-	-	-	-	-
mN1b	-	7.03	3.93	2.99	0.34	150	80	0.4	5.3	0.12	10.	0.0052	0.0034
060505 ⁴	0.089	3.93	1.72	5.13	1.15	-	-	-	-	-	-	-	-
mN2a	-	4.1	1.77	2.95	1.2	200	170	0.1	4.9	0.3	6.5	0.009	0.012
060505 _c	0.089	6.51	1.62	3.00	0.676	-	-	-	-	-	-	-	-
mN2b	-	6.3	1.64	2.99	0.6	200	170	0.1	6.4	0.2	7.0	0.005	0.07
031203 ^{5,6}	0.105	1.06	8.48	2.82	0.15	-	-	-	-	-	-	-	-
mN3	-	1.5	8.4	2.9	0.17	170	250	1.3	4.5	0.15	7.7	0.88	0.19
060614 ⁷	0.125	4.15	2.2	3.1	<0.2	-	-	-	-	-	-	-	-
mN4	-	4.4	2.2	2.95	0.24	190	170	0.12	4.7	0.1	7.	0.009	0.012
030329 ⁸	0.169	1.37	5.	3.19	0.06	-	-	-	-	-	-	-	-
mN5	-	1.45	5.	2.94	0.06	120	90	0.5	5.	0.1	6.3	0.09	0.018
120422 ⁹	0.238	4.53	2.6	4.18	0.6	-	-	-	-	-	-	-	-
mN6a	-	4.6	2.65	2.95	0.6	190	170	0.12	4.8	0.25	7.5	0.0095	0.012
120422 _c	0.238	6.19	2.5	3.00	0.43	-	-	-	-	-	-	-	-
mN6b	-	6.2	2.53	2.96	0.42	190	170	0.12	6.1	0.15	7.7	0.0069	0.0093
050826 ¹⁰	0.296	2.89	1.73	3.09	0.52	-	-	-	-	-	-	-	-
mN7	-	2.9	1.8	2.94	0.58	160	250	0.3	4.9	0.3	5.5	0.015	0.026
130427A ¹¹	0.340	2.91	2.47	4.15	0.62	-	-	-	-	-	-	-	-
mN8a	-	2.9	2.44	2.94	0.58	160	250	0.3	5.6	0.4	5.5	0.02	0.033
130427A _c	0.340	3.94	2.38	3.00	0.44	-	-	-	-	-	-	-	-
mN8b	-	3.93	2.3	2.94	0.6	160	250	0.3	6.2	0.3	6.0	0.012	0.022
130427A ¹²	-	4.2	1.8	3.	0.3	-	-	-	-	-	-	-	-
mN9	-	4.1	1.8	2.96	0.46	160	250	0.36	5.8	0.2	6.6	0.008	0.016
061021 ¹³	0.346	3.2	4.2	3.8	<0.52	-	-	-	-	-	-	-	-
mN10	-	3.4	4.1	3.	0.54	120	280	0.6	5.8	0.2	7.6	0.016	0.034
011121 ^{14,15}	0.362	3.38	1.95	3.83	0.17	-	-	-	-	-	-	-	-
mN11	-	3.2	1.98	2.94	0.19	160	250	0.3	5.3	0.1	5.5	0.015	0.026
1207149 ¹⁶	0.398	3.92	4.24	3.	0.24	-	-	-	-	-	-	-	-
mN12	-	3.73	4.25	3.	0.26	120	280	0.6	6.2	0.14	7.6	0.016	0.035

¹ in $\text{erg cm}^{-2} \text{s}^{-1}$ (calculated at the nebula); ² Christensen et al (2008); ³ the subscript c refers to the corrected line ratios; ⁴ Thöne et al (2008); ⁵ Prochaska et al (2004); ⁶ Sollerman et al (2005); ⁷ Niino et al (2016); ⁸ Levesque et al (2010a); ⁹ Schulze et al (2014); ¹⁰ Levesque et al (2010b); ¹¹ Niino et al (2016); ¹² Krüler et al (2015); ¹³ Krüler et al (2015); ¹⁴ Garnavich et al (2003); ¹⁵ Graham & Fruchter (2013); ¹⁶ Krühler et al (2015);

lower limits. Moreover, less consistent results are obtained comparing the data with diagnostic diagrams calculated for general cases. For spectra rich in number of lines from different elements in various frequency ranges, the CLOUDY, SUMA and other codes were assembled. SUMA accounts for both the photoionization and the shock because 1) it was noticed that lines from recombined elements and from very high ionization levels could not be reproduced consistently using photoionization alone, 2) the radio continuum shows the synchrotron power-law created by the Fermi mechanism at the shock front in most of the spectral energy distribution (SED), 3) low [OIII]5007+/[OIII] 4363 line ratios (such as observed in LINERs) could not be reproduced without the shocks and above all, because 4) in galaxies at high z , that derive mostly from mergers, shocks are created by collision, etc. By the detailed modelling method the simulated emitting clouds in the galaxy are characterized by the parameters of the shock and of the photoionization, by the element abundances, by the geometrical thickness due to fragmentation, etc. We calculate the emission lines from the gas adopting a set of the most significant input parameters. The calculation process is briefly described in the following. Some

of the parameters are suggested by the observations (e.g. the FWHM gives a hint to the shock velocity choice, the electron density is roughly deduced from the [SII] 6716/6731 doublet ratio, etc)). Moreover, some published grids of model results (Contini & Viegas 2001a,b) indicate in a general way how to choose the first set of input parameters. The lines calculated by the code are more than 200, because line emission contributes to the cooling process of the emitting gas in the recombination zone. The number of calculated lines is independent from the observations. Indeed, when only a few lines are observed the initial parameter set is less constrained. So we create a grid of models in order to reproduce the observations and to avoid degeneracy. In the modelling process, we aim to reproduce the observed line ratios for each element. Each line has a different strength which translates into the different precision by the fitting process. A minimum number of significant lines ([OIII] 5007+, [OII]3727+, [OIII]4363, [NII], $H\alpha$, $H\beta$) is necessary to constrain the model. We deal with line ratios to avoid distance and morphological effects. A perfect fit of the observed line ratios is not realistic because the observed data have errors, both random and systematic. The set of parameters which leads

to the best fit of the observed line ratios and continuum SED, is regarded as the result of modelling. The results are acceptable when the observed strongest line ratios are reproduced within 10%, and the weakest by $\sim 50\%$.

2.2 Brief description of the calculations

By the SUMA code (Contini 2015 and references therein) line and continuum emissions from the gas are calculated consistently with dust-reprocessed radiation in a plane-parallel geometry. The calculations start at the shock front where the gas is compressed and thermalized adiabatically, reaching the maximum temperature in the immediate post-shock region ($T(K) \sim 1.5 \times 10^5 (V_s/100 \text{ km s}^{-1})^2$, where V_s is the shock velocity). T decreases downstream following the cooling rate. The input parameters such as V_s , the atomic preshock density n_0 and the preshock magnetic field B_0 (for all models $B_0=10^{-4}$ Gauss is adopted) define the hydrodynamical field. They are used in the calculations of the Rankine-Hugoniot equations at the shock front and downstream. They are combined in the compression equation which is resolved throughout each slab of gas in order to obtain the density profile downstream. The input parameters that represent the primary radiation from the host starburst (SB) are the effective temperature T_* and the ionization parameter U . A pure black-body radiation referring to T_* is a poor approximation for a starburst, even adopting a dominant spectral type (see Rigby & Rieke 2004). However, it is the most suitable because the line ratios that are used to indicate T_* also depend on metallicity, electron temperature, density, ionization parameter, the morphology of the ionized clouds, and, in particular, they depend on the hydrodynamical field. The primary radiation source is independent but it affects the surrounding gas. In contrast, the secondary diffuse radiation is emitted from the slabs of gas heated by the radiation flux reaching the gas and collisionally by the shock. In our model the gas region surrounding the radiation source is not considered as a unique cloud, but as an ensemble of fragmented filaments. The geometrical thickness of these filaments is an input parameter of the code (D) which is calculated consistently with the physical conditions and element abundances of the emitting gas. Primary and secondary radiations are calculated by radiation transfer throughout the slabs downstream. The fractional abundances of the ions are calculated resolving the ionization equations for each element in each ionization level. The dust-to-gas ratio (d/g) and the abundances of He, C, N, O, Ne, Mg, Si, S, A, Fe, relative to H, are also accounted for. The uncertainty in the calculations is due to the atomic parameters (within 10 %) which are often updated.

3 NIINO ET AL (2016) SAMPLE GALAXIES

Niino et al presented spectroscopy results for three LGRB host galaxies at $z \leq 0.41$, observed with Gemini Multi-Object Spectrograph (Hook et al (2004), together with data collected from the literature. Some galaxy hosts were previously observed, but new data were presented by Niino et al. because for GRB 060614 host the metallicity measurements were uncertain. Therefore, it was revisited by GMOS-South spectroscopy. GRB 130427A host emission lines were already

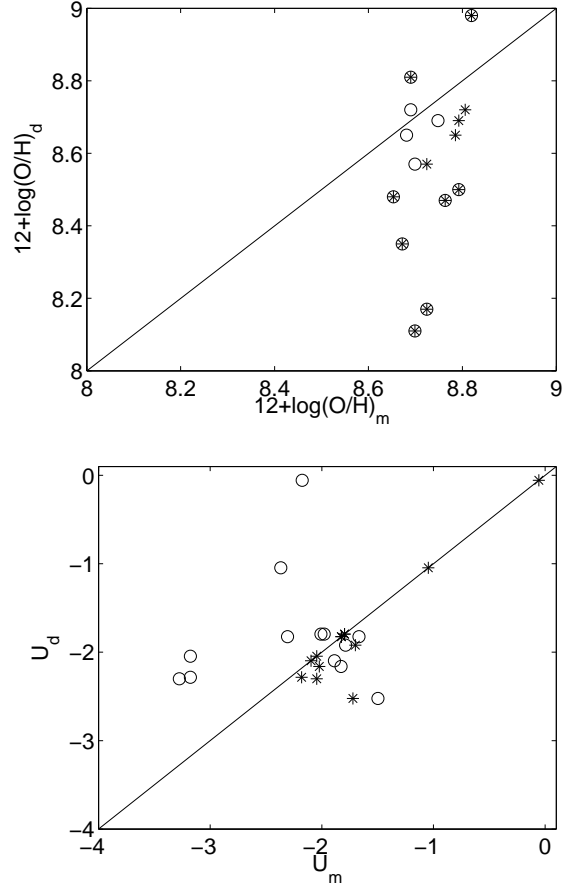


Figure 1. Top : comparison of $12+\log(\text{O}/\text{H})$ calculated by detailed modelling (m) with those calculated using indirect diagnostic calibrations (R23, N2) by Niino et al (d). Bottom : comparison of U calculated by detailed modelling (m) with those calculated by Niino et al (d). open circles: model calculations; asterisks: model calculations referring to reddening corrected data

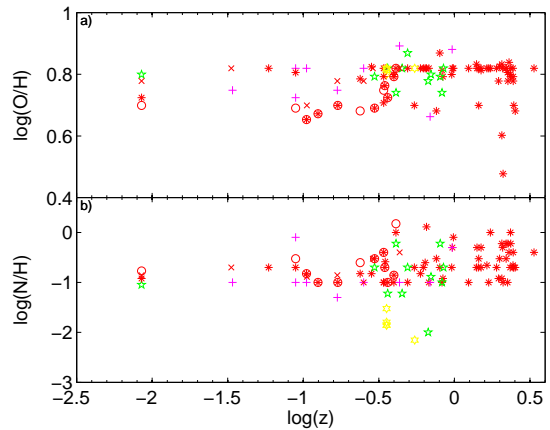


Figure 2. Calculated $\log(\text{O}/\text{H})$ (top) and $\log(\text{N}/\text{H})$ (bottom) (in units of 10^{-4} , see Table 1) as a function of z on an extended z range : symbols as in Fig. 1. Moreover, green stars : LGRB (Krühler et al); yellow hexagams : SGRB (de Ugarte Postigo et al); magenta plus : LGRB with WR stars (Han et al).

reported by Xu et al (2013) and Krühler et al (2015), but the [NII] detection was marginal in both. The host was revisited by Subaru/FOCAS. GRB 111225A host has been analyzed by archival data (Thöne & de Ugarte Postigo 2014) but they were not reported. The host was revisited with Subaru/FOCAS spectroscopy. Recently, Perley et al (2016) suggested that GRB 020819B host at $z=0.410$ reported by Niino et al happens to lie close to the line of sight of GRB020819B at $z=1.9621$, but it is entirely unrelated to the GRB. So it was removed from the modelling list.

In Table 1 we compare the calculated with the observed line ratios from Niino et al table 5. The observed line spectra were corrected for foreground Galaxy extinction. The theoretical $H\alpha/H\beta$ line ratios at the emitting nebula should be ~ 3 , considering that the emitting gas has a distribution of densities and temperatures in the recombination zone downstream of the shock front, and behind the ionization front created by the radiation source. For some galaxies in the Niino et al sample the observed $H\alpha/H\beta$ are ≥ 4 , reaching even values ≥ 5.15 and 5.5 for 060505 and 020819B, respectively. Such high $H\alpha/H\beta$ values can be found in high density gas ($> 10^6 \text{ cm}^{-3}$) where some self-absorption occurs in the Balmer lines (Osterbrock 1974). This leads to the strengthening of the $H\alpha$ line relatively to the other lines of the Balmer series (see also Contini 2003). For the forbidden lines, in particular [OII], [SII] etc. the critical densities for collisional deexcitation are $\geq 4 \times 10^3 \text{ cm}^{-3}$ and for the [OIII] 5007+ lines $\sim 6.5 \times 10^5 \text{ cm}^{-3}$, therefore high density gas in the host galaxies could be revealed by relatively strong permitted lines and abnormally high $H\alpha/H\beta$ ratios. Alternatively, considering that the line fluxes are affected by gas and dust through their path to Earth, the data should be further reddening corrected. In Table 1 first column the identification number of the galaxies is given followed by the redshift and by the line ratios presented in the different surveys, reported by Niino et al. In the rows next to those referring to observations, the best fitting calculated line ratios and the parameters adopted in the selected models are given in columns 3-6 and columns 7-13, respectively. In the last column of Table 1 the $H\beta$ line fluxes calculated at the nebula are reported. For galaxies 980425, 060505, 120422, 130427A and 020819B, we present both the data given by Niino et al and those reddening corrected (e.g. 980425_c). Models mN1, mN2, mN6, mN8 and mN13 split into e.g. mN1a and mN1b, where the former refers to Niino et al data and the latter to the corrected line ratios.

The results of modelling give shock velocities between 120 and 200 km s^{-1} , pre-shock densities between 80 and 280 cm^{-3} , in agreement with previous results obtained for a large sample of LGRB hosts (Contini 2016). Except for 060614, for all the galaxies the geometrical thickness of the emitting clouds is ≤ 0.2 pc. The physical conditions of the gas emitting the Balmer lines show $\tau \leq 1$. There is a rough agreement for U calculated from modelling the reddening corrected spectra and $U=q/c$ determined on the basis of strong-line methods (Kobulnicky & Kewley 2004) applied, however, to underreddened line ratios by Niino et al (Fig. 1, bottom diagram). The reddening corrected [OII]/[OIII] line ratios are higher than those presented by Niino et al, implying models with higher star temperatures, higher O/H and lower U , because these parameters affect differently the [OII]/ $H\beta$ and [OIII]/ $H\beta$ line ratios. The O/H metallicities

calculated by the detailed modelling and by the strong-line method are compared in Fig. 1 (top diagram). The uncertainty in the Niino et al metallicity is ~ 0.1 . A rough agreement is seen for $12+\log(\text{O}/\text{H}) > 8.65$ considering the approximation for both the strong-line methods and the detailed modelling.

Even if higher O/H are predicted by the detailed modelling than by the strong-line methods, with O/H between Allen solar value (6.6×10^{-4}) and the Asplund et al. one (4.9×10^{-4}), the O/H relative abundances calculated to fit the Niino et al corrected line ratios are all lower than solar. This would imply that O/H ratios calculated by detailed modelling for the LGRB host sample at $z < 0.41$ are lower than those (mostly solar) calculated by Contini (2016) for higher z objects by a factor ≤ 2 , as shown in Fig. 2. A few LGRB hosts with $\text{O}/\text{H} \leq 4.9 \times 10^{-4}$ could be seen as minima throughout the z range. The O/H ratios recover solar values towards local galaxies. Considering that lower than solar metallicities derive from mixing with external matter during galaxy merging, it seems that the merging process is highly efficient at low z .

4 THE SPECTRA IN THE DIFFERENT REGIONS OF LGRB 980425 HOST GALAXY

Niino et al report the average spectrum of the LGRB 980425 host galaxy presented by Christensen et al in table 2, last row. The uncertainties are very large in the line flux means, therefore in the following we refer to the single region spectra.

4.1 Modelling Christensen et al (2008) data

In Tables 2 and 3 we present the modelling of the spectra observed throughout the 980425 host and the selected models which best reproduce the observed line ratios. The data were obtained by the Very Large Telescope UT3 Melipal with the VIMOS integral field spectroscopy mode. In Table 2 the line ratios reported by Christensen et al are shown in columns 2-7 followed by the reddening corrected line ratios in columns 9-14. In the next rows the calculated line ratios best fitting the data (models mc1-mc26) and best fitting the corrected line ratios (models m1c-m26c) are reported. The models are described in Table 3. Most of the observed $H\alpha/H\beta$ are > 3 . As discussed in Sect. 3, the pre-shock densities and the geometrical thickness used by models mc1-mc26 yield optical thickness $\tau < 1$, therefore we have corrected for reddening the line ratios. In Fig. 3 (top diagram) the observed $H\alpha/H\beta$ are given as function of the observed [OII]/ $H\beta$. The three observed spectra corresponding to models mc6, mc11 and mc17 show $H\alpha/H\beta = 12.7, 10.4$ and 11.9 , respectively. The correction factor is very high and leads to high corrected [OII]/ $H\beta$, in particular for the latter, which corresponds to an already high uncorrected [OII]/ $H\beta$. High [OII]/ $H\beta$ are generally found in collisionally dominated nebulae, suggesting that shocks are at work. The $H\alpha/H\beta$ ratios for the two former spectra (referring to mc6 and mc11) correspond to relatively low [OII]/ $H\beta$ indicating that the reddening correction makes sense. The [OIII]/ $H\beta$ versus [OII]/ $H\beta$ corrected and not-corrected line ratios (Fig. 3 bottom diagram) show that even if the trend corresponds to a radiative situation

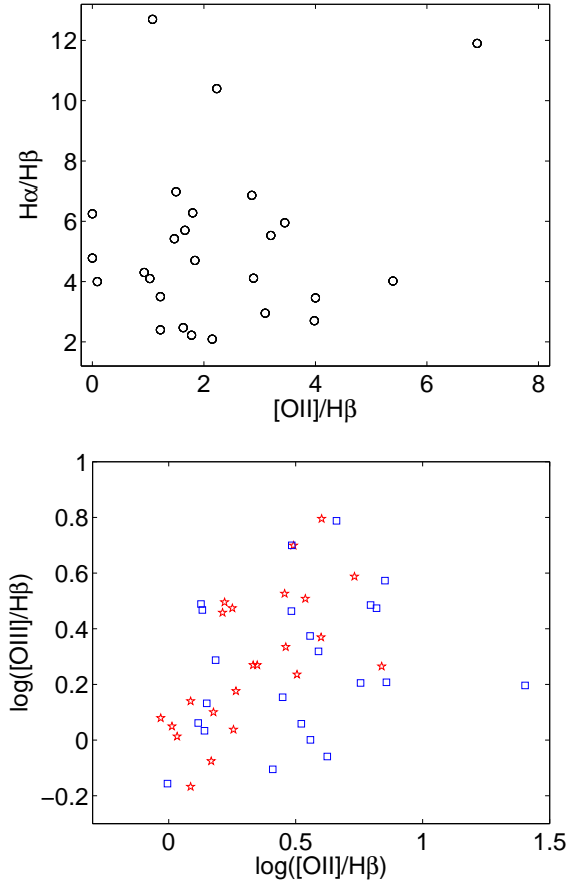


Figure 3. Christensen et al data. Top : observed $H\alpha/H\beta$ versus observed $[OIII]/H\beta$. Bottom : observed $[OIII]/H\beta$ versus $[OII]/H\beta$ (red pentagrams); corrected $[OIII]/H\beta$ versus $[OII]/H\beta$ (blue squares)

with small U (Contini 2016, fig. 1), the data are scattered, confirming that another mechanism, e.g. the shocks cannot be neglected.

Table 3 shows that the $H\beta$ flux calculated at the emitting nebula is relatively high in the WR star region, and the same should be for $H\alpha$ ($\sim 3 H\beta$) confirming a relatively high SFR. Metallicities in terms of O/H and N/H relative abundances are close to solar. In the extreme east, in the host regions at $10.1'' \times 8.0''$ and $14.8'' \times 3.3''$ O/H drops to minima of $4. \times 10^{-4}$ and $5. \times 10^{-4}$, respectively. Fig. 4 shows that O/H values calculated by detailed modelling exceed those obtained by Christensen et al. using the strong-line method by a factor >2 . Table 3 shows that sulphur is almost underabundant everywhere ($(S/H)_{\odot} = 2. \times 10^{-5}$). S is easily trapped into dust grains and subtracted from the gaseous phase by factors <10 .

Following Christensen et al we present our results in the maps of Fig. 5. We refer to pre-shock densities, star temperatures, ionization parameters and observed $H\alpha/H\beta$. We have chosen the symbols showing darker areas with increasing parameter in each diagram. They are described in Table 4. Fig. 5 shows the following features. T_* increases towards the south-west zone and reaches $T_* = 8.4 \times 10^4 K$ in the SN region, slightly lower than $T_* > 10^5 K$ which was

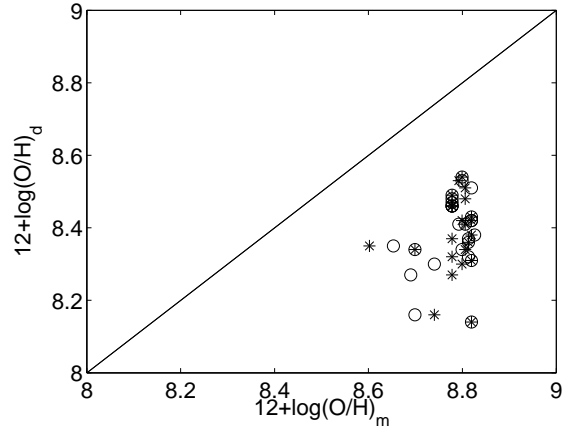


Figure 4. Comparison of $\log(O/H)+12$ calculated by detailed modelling (m) with those calculated using indirect diagnostic calibrations by Christensen et al (d). open circles: model calculations; asterisks: model calculations referring to reddening corrected data.

calculated by Contini (2016) modelling the Han et al (2010) survey. Han et al suggest that WR and O stars are present in some LGRB (e.g. 980703, 990712) and in other host galaxies (Contini 2016, table 10). The ionization parameter has an opposite trend. A diluted U in the SN region indicates that the radiation source is far from the emitting gas or that the photoionizing flux is prevented from reaching the gas by obstructing matter. The $H\alpha/H\beta$ observed line ratio is <3 in the WR zone indicating that it is not affected by dust absorption. On the other hand, in the SN region the line fluxes require a reddening correction. The preshock densities are relatively low throughout the whole galaxy, except in the north-east zone where $n_0 > 300 \text{ cm}^{-3}$ are revealed. The densities inside the gaseous clouds increase by a factor >4 due to compression downstream.

We have found that the line spectrum observed from the host region $2.7'' \times -4.0''$ in GRB 980425 is reproduced adopting an accretion model, in agreement with Michalowski et al (2016) who claim that accretion is more adapted than outflow in starburst galaxies. Michalowski et al recently published [CII] $158\mu\text{m}$ and [OI] $63\mu\text{m}$ line fluxes in the FIR. They claim that [CII] emission exhibits a normal radial profile while [OI] is concentrated close to the WR zone. We have calculated the [CII] and [OI] line fluxes consistently with the optical lines using the same models (Table 3) in each region. Our results (Table 5, Fig. 5) show that [OI] are weak throughout the host with higher values in the regions within a band roughly oriented from north-east to south-west. For [CII] the radial structure can be roughly recognized. In the WR and SN regions, the calculated values are within the mean, suggesting that clouds different from those emitting the optical lines contribute to the FIR emission lines. According to the results presented for the LGRB 031203 host galaxy in Sect. 5., they could be represented by shock dominated ($U=0$) filaments, but the data are not enough to constrain the models.

Table 2. Modelling [OII]3727+, [OIII]5007+, H α , [NII]6583, [SII]6717, 6731 line ratios to H β =1 from GRB 980425 host regions (Christensen et al 2008)

	[OII]/ H β	[OIII]/ H β	H α / H β	[NII]/ H β	[SII]/ H β	[SII]/ H β		[OII]/ H β	[OIII]/ H β	H α / H β	[NII]/ H β	[SII]/ H β	[SII]/ H β
galaxy	5.39	3.87	4.02	0.44	0.63	0.15		7.1	3.74	3.	0.33	0.45	0.11
mc1	5.41	3.97	2.97	0.44	0.58	0.66	m1c	7.2	3.8	3.	0.39	0.45	0.5
WR region	4.	6.24	3.46	0.27	0.3	0.23		4.57	6.14	3.	0.23	0.25	0.2
mc2	4.	6.24	2.94	0.3	0.27	0.3	m2c	4.5	6.18	3.	0.3	0.26	0.3
SN region	3.45	3.22	5.95	0.67	1.22	0.91		6.6	3.	3.	0.34	0.56	0.4
mc3	3.4	3.2	2.96	0.68	0.78	0.9	m3c	6.7	3.2	3.	0.36	0.54	0.6
WR(-8.7)	3.1	5.	2.95	0.21	0.21	0.17		3.	5.	3.	0.21	0.21	0.17
mc4	3.	5.2	2.95	0.2	0.27	3.	m4c	3.	5.2	3.	0.22	0.27	0.32
SN(-5.3)	2.86	3.36	6.86	0.82	1.53	1.12		6.24	3.	3.	0.36	0.59	0.42
mc5	2.79	3.33	2.96	0.86	0.83	0.9	m5c	6.4	3.1	3.	0.24	0.53	0.56
(-11.4)	1.08	1.03	12.7	0.146	2.	1.52		4.2	0.87	3.	0.034	0.38	0.28
mc6	1.1	1.01	2.99	0.17	1.3	1.5	m6c	4.3	0.86	3.	0.1	0.35	0.38
(-8.0)	1.8	1.09	6.28	1.08	1.65	1.29		3.6	1.	3.	0.52	0.71	0.54
mc7	1.8	1.12	3.	0.9	1.64	1.7	m7c	3.86	1.	3.	0.6	0.7	0.7
(-6.7)	1.5	1.26	6.98	0.86	1.22	1.04		3.3	1.1	3.	0.37	0.46	0.39
mc8	1.7	1.25	3.	0.8	1.23	1.29	m8c	3.4	1.19	3.	0.4	0.48	0.49
(-4.0)	1.84	1.5	4.7	0.59	0.73	0.53		2.81	1.42	3.	0.37	0.44	0.3
mc9	1.9	1.5	2.98	0.6	0.6	0.62	m9c	2.97	1.4	2.98	0.36	0.45	0.46
(-2.0)	3.2	1.72	5.53	0.78	0.94	0.77		5.7	1.6	3.	0.42	0.47	0.37
mc10	3.	1.77	2.98	0.7	0.8	0.73	m10c	5.88	1.6	3.	0.4	0.47	0.42
(-1.3,-6.1)	2.23	1.86	10.4	1.2	1.84	1.29		7.2	1.6	3.	0.35	0.44	0.3
mc11	2.1	1.92	3.	0.9	1.42	1.22	m11c	7.4	1.6	3.1	0.46	0.42	0.35
(-1.3,10.0)	1.47	0.84	5.42	0.76	1.06	0.86		2.56	0.78	3.	0.42	0.53	0.43
mc12	1.5	0.84	3.	0.7	1.07	0.93	m12c	2.57	0.82	3.	0.43	0.58	0.5
(-0.7)	2.89	2.16	4.11	0.53	0.43	0.3		3.89	2.08	3.	0.38	0.3	0.2
mc13	2.96	2.02	3.	0.66	0.46	0.39	m13c	3.7	2.1	3.	0.4	0.3	0.26
(-0.0)	1.66	3.13	5.7	0.92	1.23	0.92		3.0	2.9	3.	0.48	0.59	0.43
mc14	1.67	3.1	3.	0.9	1.04	1.04	m14c	3.1	2.97	3.	0.6	0.59	0.58
(2)	0.0	0.99	6.25	0.87	1.5	1.28		0.0	0.91	3.	0.42	0.65	0.54
mc15	0.7	1.0	3.	0.7	0.65	1.18	m15c	0.8	0.96	2.97	0.48	0.46	0.85
(2.7)	1.03	1.12	4.1	0.61	0.66	0.44		1.38	1.08	3.	0.44	0.46	0.30
mc16	1.02	1.13	3.05	0.63	0.47	0.51	m16c	1.34	1.18	3.	0.4	0.36	0.4
(2.7,-4.0)	6.9	1.84	11.9	0.44	0.62	0.4		25.	1.57	3.	0.44	0.62	0.41
mc17	7.0	1.84	3.17	1.8	2.6	2.2	m17c	25.6	1.4	3.25	0.42	0.55	0.56
(5.4)	0.93	1.2	4.3	0.63	0.77	0.56		1.3	1.15	3.	0.44	0.51	0.37
mc18	0.91	1.25	3.05	0.5	0.74	0.79	m18c	1.45	1.1	3.1	0.46	0.57	0.57
(6.1)	1.22	1.38	3.5	0.53	0.76	0.54		1.4	1.35	3.	0.45	0.64	0.45
mc19	1.1	1.4	3.05	0.6	0.77	0.8	m19c	1.3	1.35	3.	0.48	0.52	0.47
(8.7)	1.22	0.68	2.4	0.31	0.68	0.42		0.99	0.7	3.	0.39	0.88	0.54
mc20	1.21	0.63	3.	0.4	0.7	0.6	m20c	1.04	0.7	3.	0.3	0.7	0.58
(9.4)	1.63	2.87	2.47	0.27	0.4	0.3		1.36	2.93	3.	0.33	0.5	0.38
mc21	1.75	2.9	2.99	0.4	0.44	0.44	m21c	1.4	2.85	3.	0.32	0.4	0.42
(10.1)	0.09	2.45	4.	0.49	0.68	0.48		0.12	2.37	3.	0.37	0.49	0.34
mc22	0.12	2.47	3.	0.1	0.02	0.03	m22c	0.23	2.2	3.	0.4	0.4	0.5
(11.4)	1.78	2.98	2.22	0.37	0.33	0.25		1.3	3.08	3.	0.5	0.46	0.35
mc23	1.8	2.97	2.99	0.38	0.37	0.37	m23c	1.37	2.95	3.	0.44	0.37	0.37
(12.1)	0.00	1.3	4.78	0.67	0.9	0.77		0.0	1.23	3.	0.42	0.53	0.45
mc24	0.7	1.2	2.98	0.7	0.66	1.22	m24c	0.8	1.2	2.98	0.48	0.4	0.7
(14.8,3.3)	3.98	2.34	2.7	0.29	0.56	0.39		3.6	2.36	3.	0.47	0.66	0.61
mc25	3.99	2.24	2.95	0.3	0.38	0.5	m25c	3.67	2.3	2.95	0.4	0.45	0.6
(14.8,10.)	2.15	1.86	2.09	0.33	0.44	0.4		1.53	1.94	3.	0.47	0.66	0.61
mc26	2.3	1.94	3.	0.5	0.45	0.39	m26c	1.5	2.1	3.	0.48	0.62	0.53

4.2 Hammer et al (2006) multi-line spectra

To check whether the models calculated to reproduce the line ratios observed by Christensen et al from the SN and WR regions are able to explain the data reported by other observers, we apply the detailed modelling method to the spectroscopic VLT/FORS2 observations presented by Ham-

mer et al (2006, table 1) which contain a relatively large number of lines covering an extended range of frequencies and of elements. In Table 6 we compare model results (mSN, mWR and mrg4) with the data. The line ratios were corrected on the basis of previous considerations. However, the spectrum from region "4" is characterised by

Table 3. Models calculated to reproduce the spectra by Christensen et al (2008) reported in Table 2

	V_s km s ⁻¹	n_0 cm ⁻³	D 10 ¹⁸ cm	O/H 10 ⁻⁴	N/H 10 ⁻⁴	S/H 10 ⁻⁴	T_* 10 ⁴ K	U -	H β ¹
mc1	150	100	0.4	4.9	0.17	0.04	9.	0.0076	0.006
m1c	150	100	0.4	6.	0.14	0.03	9.4	0.0056	0.0047
mc2	150	100	0.4	5.	0.17	0.02	8.4	0.018	0.01
m2c	150	100	0.4	5.5	0.17	0.02	8.4	0.016	0.01
mc3	150	100	0.3	5.5	0.5	0.08	6.5	0.014	0.01
m3c	150	100	0.3	6.3	0.15	0.04	8.3	0.0055	0.0046
mc4	150	100	0.3	6.6	0.2	0.03	6.5	0.032	0.015
m4c	150	100	0.3	6.6	0.2	0.03	6.5	0.032	0.015
mc5	120	100	0.3	6.6	0.8	0.1	6.	0.018	0.01
m5c	120	100	0.3	6.6	1.	0.04	8.4	0.0044	0.0037
mc6	120	100	0.3	6.	0.3	0.3	3.4	0.15	0.027
m6c	120	100	0.3	6.	0.06	0.04	5.	0.003	0.003
mc7	130	80	0.3	6.6	1.	0.3	4.4	0.02	0.0084
m7c	130	80	0.3	6.4	0.4	0.08	5.	0.005	0.0034
mc8	130	80	0.3	6.4	1.	0.22	4.4	0.024	0.0095
m8c	130	80	0.3	6.4	0.3	0.06	4.8	0.008	0.0048
mc9	130	80	0.3	6.2	0.8	0.1	4.4	0.03	0.01
m9c	130	80	0.3	6.4	0.3	0.06	4.7	0.012	0.0063
mc10	120	70	0.2	6.6	0.6	0.1	5.2	0.01	0.0037
m10c	120	60	0.2	6.6	0.2	0.04	5.9	0.003	0.0015
mc11	120	50	1.	6.7	1.	0.2	5.5	0.015	0.0042
m11c	120	50	1.	6.6	0.2	0.03	7.8	0.0014	8.3e-4
mc12	120	50	2.	6.3	1.	0.2	4.4	0.015	0.0046
m12c	120	50	2.	6.2	0.4	0.08	4.8	0.0055	0.0026
mc13	120	50	2.	6.3	0.6	0.05	6.1	0.008	0.0032
m13c	120	50	2.	6.4	0.3	0.03	6.4	0.006	0.0027
mc14	120	80	2.	6.5	1.2	0.14	6.1	0.03	0.013
m14c	120	80	2.	6.5	0.5	0.06	7.	0.01	0.0067
mc15	130	320	0.1	6.0	1.4	0.3	3.0	0.8	0.22
m15c	130	320	0.1	6.0	0.8	0.2	2.9	0.9	0.23
mc16	120	100	5.5	6.0	1.	0.1	4.5	0.03	0.02
m16c	120	100	5.5	6.0	0.7	0.07	4.6	0.025	0.019
mc17	120	50	0.17	6.6	1.	0.26	5.8	8.e-4	4.e-4
m17c ²	54	200	0.0035	6.3	0.15	0.14	3.2	0.003	1.6
mc18	110	100	5.5	6.	1.	0.16	4.5	0.044	0.024
m18c	100	120	6.5	6.4	0.6	0.1	5.5	0.01	0.013
mc19	120	100	5.5	6.	1.	0.15	4.6	0.04	0.022
m19c	120	100	5.5	6.	0.7	0.1	5.0	0.02	0.017
mc20	120	50	5.	6.3	0.6	0.15	4.2	0.016	0.006
m20c	120	50	5.	6.3	0.6	0.15	4.	0.03	0.008
mc21	120	80	2.	6.5	0.6	0.06	5.6	0.033	0.0124
m21c	120	80	2.	6.	0.5	0.06	5.2	0.059	0.016
mc22	100	200	0.1	4.5	2.	0.3	4.	0.95	0.058
m22c	100	160	2.	4.	2.	0.09	3.9	9.4	0.11
mc23	120	80	2.	6.5	0.5	0.05	5.6	0.033	0.012
m23c	120	80	4.	6.	0.6	0.05	5.8	0.042	0.015
mc24	130	320	0.1	6.	1.4	0.3	3.1	0.83	0.22
m24c	130	320	0.1	6.	0.8	0.16	3.	0.83	0.22
mc25	150	140	0.18	5.	0.14	0.04	6.3	0.0094	0.01
m25c	150	140	0.18	5.	0.2	0.05	6.1	0.011	0.01
mc26	120	50	1.	6.6	0.6	0.06	5.3	0.015	0.0042
m26c	120	50	1.	6.6	0.6	0.09	4.9	0.015	0.0043

¹ in erg cm⁻² s⁻¹ (calculated at the nebula); ² calculated by an infalling model.

a relatively low H β flux, leading to H α /H β = 8.217. The observed [OII]/H β = 11.65 skips to 30 by reddening correction, which looks very high. We reproduce it by \sim 40% adopting a very low U (0.0004). The [OIII] 4363/H β is over-predicted by $>$ 50% by model mrg4. This suggests that the abnormally high H α /H β is not only due to dust absorp-

tion, but some self absorption across high density gas has reduced the H β flux reported by Hammer et al in their table 1. [ArIII]7136/H β observed from region "4" is well reproduced by model mrg4, while [ArIII]7136/H β data from the WR and SN regions are under-predicted by the models by a factor of \sim 3, adopting Ar/H = 3.3×10^{-6} .

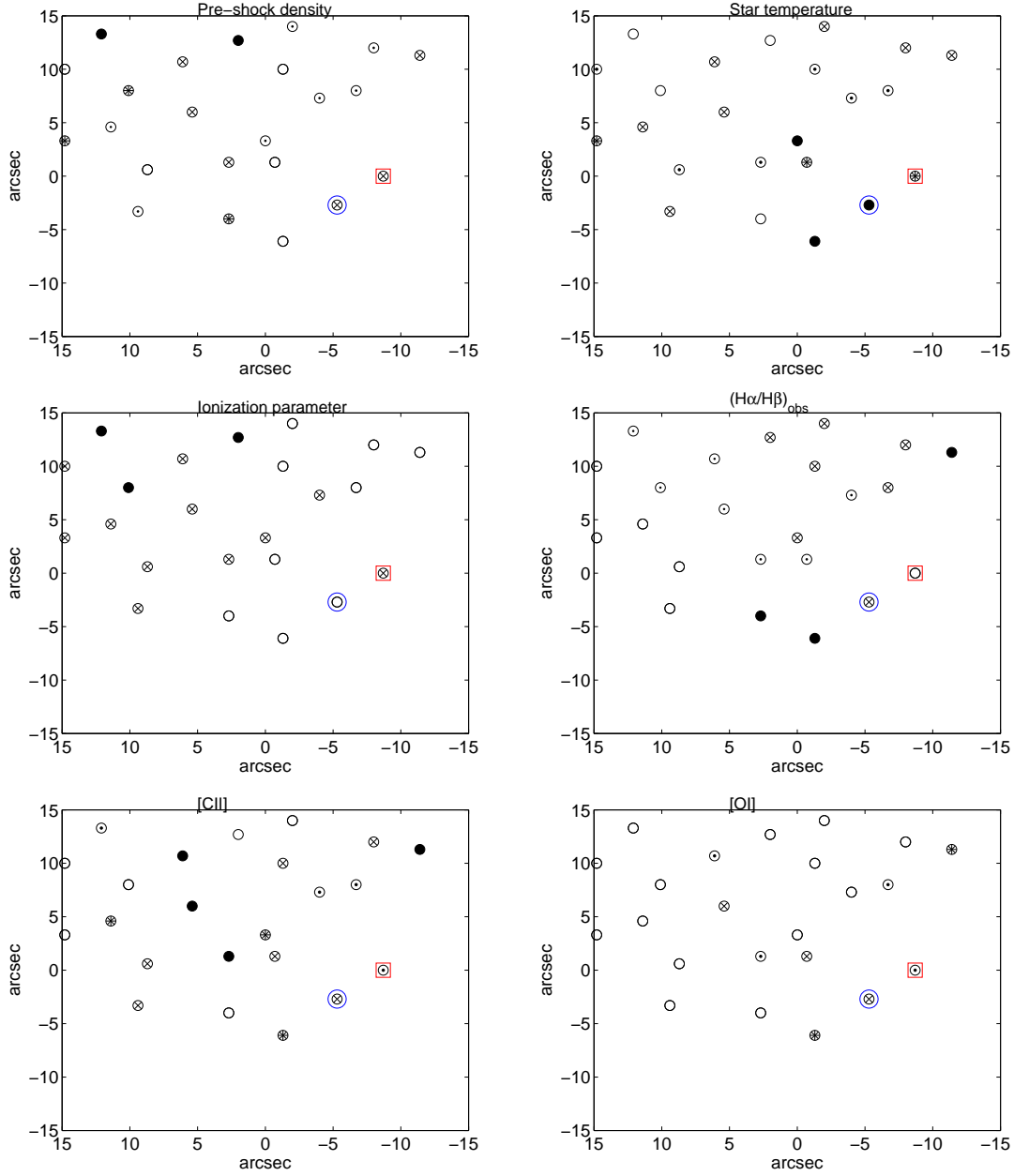


Figure 5. Christensen et al data. Distribution of the physical parameters throughout the galaxy GRB 980435 host. n_0 (top left); T_* (top right); U (middle left); $(H\alpha/H\beta)_{obs}$ (middle right); $[CII]158\mu m$ flux calculated at the nebula (bottom left); $[O]63\mu m$ flux calculated at the nebula (bottom right); large blue circle : the SN place and large red square : the region where WR stars were detected. Symbols relative to the different parameters are explained in Table 4.

Table 4. Symbols in Fig. 5 diagrams

	left-top n_0 cm^{-3}	right-top T_* $10^4 K$	left-middle U -	right-middle $(H\alpha/H\beta)^1$ -	left-bottom [CII] line flux ² $0.01 \text{ erg cm}^{-2} \text{ s}^{-1}$	right-bottom [O] line flux ² $0.01 \text{ erg cm}^{-2} \text{ s}^{-1}$
open circle	50	<4.	<0.01	<3	≤ 0.1	≤ 0.1
encircled dot	60-80	4.-4.9	-	3-5	0.1-0.2	0.1-0.2
encircled cross	100-120	5.-5.9	0.01 -0.1	5-7	0.2-0.4	0.2-0.5
encircled asterisk	140-200	6.-6.5	-	-	0.4-0.9	0.5-1
black circle	320	≥ 7	>0.1	>10	>0.9	-

¹ observed at Earth; ² calculated at the nebula

Table 5. Flux (in $0.01 \text{ erg cm}^{-2} \text{ s}^{-1}$) of [CII] and [OI] lines calculated at the nebula by the m4c-m26c models (Table 3)

model	[CII]158 μm	[OI]63 μm	model	[CII]158 μm	[OI]63 μm
m4c	0.11	0.207	m16c	1.80	0.098
m5c	0.29	0.430	m17c	0.002	0.000
m6c	1.03	0.972	m18c	3.29	0.384
m7c	0.21	0.015	m19c	1.34	0.099
m8c	0.161	0.161	m20c	0.438	0.034
m9c	0.120	0.009	m21c	0.360	0.033
m10c	0.074	0.009	m22c	0.09	0.018
m11c	0.588	0.588	m23c	0.72	0.07
m12c	0.403	0.030	m24c	0.176	0.0220
m13c	0.269	0.235	m25c	0.028	0.0074
m14c	0.871	0.062	m26c	0.105	0.0075
m15c	0.176	0.022	-	-	-

Table 6. Modelling the line spectra from Hammer et al (2006, table 2)

	SN	SN (corr)	mSN	WR	WR (corr)	mWR	reg 4	reg 4 (corr)	mrq4
[OII] 3727	4.44	6.23	6.7	1.24	2.08	3.	11.65	30.13	17.4
[NeIII] 3869	0.61	0.81	0.68	0.32	0.49	0.49	0.239	0.53	0.66
[OIII] 4363	<0.033	0.039	0.04	0.044	0.055	0.02	0.13	0.20	0.58
[NIII] 4640	0.00	0.00	-	0.008	0.01	-	0.00	0.00	-
HeII 4686	<0.055	0.056	0.05	0.015	0.015	0.02	0.00	0.00	0.01
[ArIV] 4711	0.00	0.000	0.0035	0.01	0.009	0.001	0.00	0.00	0.05
[ArIV] 4740	0.00	0.000	0.0026	0.004	0.004	0.001	0.00	0.00	0.04
H β 4861	1.	1.	1.	1.	1.	1.	1.	1.	1.
[OIII] 5007+	3.26	3.13	3.06	7.06	6.63	5.26	7.26	6.5	7.27
[NII] 5755	0.00	0.000	0.011	0.005	0.004	0.003	0.00	0.00	0.05
[OI] 6300+	0.44	0.33	0.47	0.048	0.03	0.16	0.869	0.37	0.084
[SIII] 6312	0.04	0.03	0.002	0.025	0.016	0.001	0.00	0.00	0.053
[NII] 6548	0.42	0.3	0.36	0.118	0.069	0.1	1.478	0.55	0.43
H α 6563	4.28	3.	3.	5.19	3.	2.95	8.217	3.	3.
[NII] 6584	0.98	0.68	0.72	0.32	0.18	0.26	2.26	0.8	0.84
[SII] 6716	0.66	0.44	0.54	0.31	0.16	0.27	2.35	0.74	0.79
[SII] 6731	0.93	0.61	0.57	0.24	0.128	0.3	2.56	0.79	0.66
[ArIII]7136	0.21	0.14	0.04	0.22	0.114	0.03	0.41	0.12	0.14
[OII] 7325	0.21	0.13	0.2	0.009	0.041	0.09	0.548	0.13	1.
[ArIII] 7751	0.0	0.02	-	0.006	0.026	-	0.00	0.00	-
V_s (km s $^{-1}$)	-	-	120	-	-	150	-	-	140
n_0 (cm $^{-3}$)	-	-	100	-	-	100	-	-	40
$D(10^{18} \text{cm})$	-	-	0.3	-	-	0.3	-	-	0.02
T_* (10 4 K)	-	-	8.	-	-	6.5	-	-	4.6
U	-	-	0.004	-	-	0.032	-	-	4e-4
He/H	-	-	0.1	-	-	0.1	-	-	0.1
N/H (10 $^{-4}$)	-	-	0.3	-	-	0.2	-	-	0.5
O/H (10 $^{-4}$)	-	-	6.6	-	-	6.6	-	-	7.0
Ne/H (10 $^{-4}$)	-	-	1.	-	-	1.	-	-	0.7
S/H (10 $^{-4}$)	-	-	0.04	-	-	0.06	-	-	0.15
Ar/H(10 $^{-4}$)	-	-	0.033	-	-	0.033	-	-	0.033
H β (erg cm $^{-2}$ s $^{-1}$) at the nebula	-	-	0.0037	-	-	0.015	-	-	1.e-4

5 LGRB 031203 OPTICAL AND MID-IR LINES

The lines in the optical range from GRB 031203 host galaxy were observed and modelled in different ways in the last years (Niino et al and references therein, Contini 2016, etc). We have reproduced the line ratios by the radiation dominated (RD) mN3 model (Table 1), characterized by relatively low O/H and N/H and a relatively high T_* . The model accounts consistently also for the shock.

Recently, Watson et al (2016) presented the first mid-

IR spectrum of a GRB host (HG031203) by low and high resolution spectroscopy with *Spitzer-IRS*. Watson et al found that the IRS spectra show strong high ionization fine structure emission lines such as [SIV] 10.51 μm which suggest a hard radiation field in the galaxy and therefore strong ongoing star formation and a very young stellar population. They claim that the absence of PAH supports this idea as well as the hot dust peak temperature. We remind that high ionization lines are strong in presence of the shocks which heat the gas to temperatures \propto

$(V_s)^2$. Moreover, PAH grains are very small ($< 0.01 \mu\text{m}$) and easily sputtered throughout the shock front. We refer to the observed $[\text{SIV}]10.51\mu\text{m} / [\text{SIII}]18.71\mu\text{m}$ ($=1.63$) and $[\text{NeIII}]15.56\mu\text{m} / [\text{NeII}]12.81\mu\text{m}$ ($=15.14$) line ratios. By the code SUMA line fluxes from far-UV to far-IR are calculated consistently for each model. The IR line ratios calculated by model mN3 do not reproduce the observed line ratios. On the other hand, the shock dominated (SD) model calculated adopting the same shock input parameters as mN3 but with $U=0$, approximates the data by an error of $\sim 50\%$ ($[\text{SIV}]/[\text{SIII}]=3.8$ and $[\text{NeIII}]/[\text{NeII}]=7$). In this case the geometrical thickness of the emitting clouds is reduced to $D=1.17 \times 10^{15}$ cm.

To better understand the results, the profiles of the electron temperature and density within the emitting clouds and of the fractional abundances of the H, O, Ne and S ions in different ionization stages are shown in Fig. 6 for both the RD (top diagrams) and the SD (bottom diagram) models. The RD model corresponds to the case in which the gas moves outwards from the starburst, therefore the photoionizing radiation reaches the edge (on the right of the right top diagram) of the cloud opposite to the shock front (on the left of the left top diagram). The emitting cloud corresponding to the RD model is divided into two halves represented by the left and right top diagrams. The left diagram shows the region close to the shock front and the distance from the shock front on the X-axis scale is logarithmic. The right diagram shows the conditions downstream far from the shock front, close to the edge reached by the photoionization flux which is opposite to the shock front. The distance from the illuminated edge is given by a reverse logarithmic X-axis scale. The two edges of the cloud are bridged by the secondary radiation from both sides. In the SD case (bottom diagram) the gas is collisionally heated by the shock and by secondary radiation emitted by the slabs of gas heated by the shock. The gas recombines in the downstream region. Fig. 6 shows that the optical lines calculated by the mN3 model are emitted from RD clouds moving outwards, while the corresponding mid-IR ones come from cloud fragments which are not reached by the primary radiation flux.

6 CONCLUDING REMARKS

We revisited the line spectra reported by Niino et al for galaxies at $z \leq 0.41$ in order to complete by the detailed modelling of the line ratios the calculation of the physical conditions and relative abundances in LGRB host galaxies in the redshift interval $0.0085 \leq z < 0.5$. Our results suggest that the high $\text{H}\alpha/\text{H}\beta$ ratios (which reach values as high as 5.5 in some of the observed spectra) cannot originate from high density gas which is not predicted by the observed $[\text{SII}]$ doublet and by strong forbidden lines in general. Therefore, the line ratios were reddening corrected. We have found in LGRB host galaxies at $z \leq 0.41$ lower metallicities than in LGRB hosts at higher z , suggesting that merging is proceeding. Detailed modelling yields higher metallicities than those calculated by the methods in most of the galaxies.

The investigation of different regions throughout the GRB 980425 galaxy at $z=0.0085$ which hosts a WR and a SN, leads Christensen et al to claim that extreme values of SFR, stellar masses etc. arise only in the WR region and

that the lowest metallicity values are found in the WR and GRB regions. The calculation method of metallicities is still a debated issue and different conclusions can be reached. By the detailed modelling of the line ratios presented in this paper we have added more information to the Christensen et al maps about metallicities and physical conditions in the different regions. In particular, we have found that the effective starburst temperature in the SN region is the highest throughout the host galaxy. A low U reveals that in the SN region the emitting gas is far from the radiation source in agreement with Fynbo et al (2000) who claim by high spatial resolution imaging, that the GRB and the associated SN did not occur in the regions where the WR stars and O stars are located, corresponding to rich and compact clusters of SFR, but several hundreds parsec away. Moreover, our results show that O/H is slightly lower than solar, N/H is lower than solar and S is depleted from the gaseous phase in nearly all the regions throughout the host. Comparison of the pre-shock density map with the $\text{H}\alpha/\text{H}\beta$ one confirms that high $\text{H}\alpha/\text{H}\beta$ are due to dust reddening rather than to self absorption by high density gas. Following Chevalier (1982) theory, two shocks are formed after the SN explosion, one propagating towards the SN and one proceeding outward throughout the ISM. We suggest that the line ratios observed by Christensen et al in the SN region are emitted downstream of the outward shock front, where the pre-shock density and the shock velocity are suitable to the ISM.

Region $2.7'' \times -4.0''$ line spectrum (Table 2) in the GRB 980425 host, which shows an abnormally high $[\text{OII}]/[\text{OIII}]$ line ratio, could be reproduced only by an accretion model, i.e. the emitting gaseous cloud is infalling towards the radiation source. Accretion rather than outflow is supported by Michalowski et al in starburst galaxies. Modelling results of $[\text{CII}] 158$ and $[\text{OI}] 63$ FIR line fluxes observed by Michalowsky et al in the SN and WR regions are similar in average to those obtained in the other regions of the host galaxy.

The models calculated for the SN and WR regions on the basis of the Christensen et al data, were constrained only by a few oxygen, nitrogen and sulphur line ratios to $\text{H}\beta$. We have checked them by modelling the line ratios observed by Hammer et al. We have found that the same models reproduce satisfactorily also the $\text{HeII}/\text{H}\beta$ and $[\text{ArIII}]/\text{H}\beta$ line ratios. High temperature stars in the SN region are confirmed.

The modelling of $[\text{SIV}]10.51/[\text{SIII}]18.71$ and $[\text{NeIII}]10.6/[\text{NeII}]12.81$ line ratios observed by Watson et al from GRB 031203 host galaxy at $z=0.105$ indicates that the mid-IR lines are emitted from geometrically thin shock dominated clouds which are not reached by the starburst photoionizing flux, while the optical lines are emitted from the radiation dominated outflowing clouds.

ACKNOWLEDGEMENTS

I am very grateful to the referee for many critical suggestions which substantially improved the presentation of the paper.

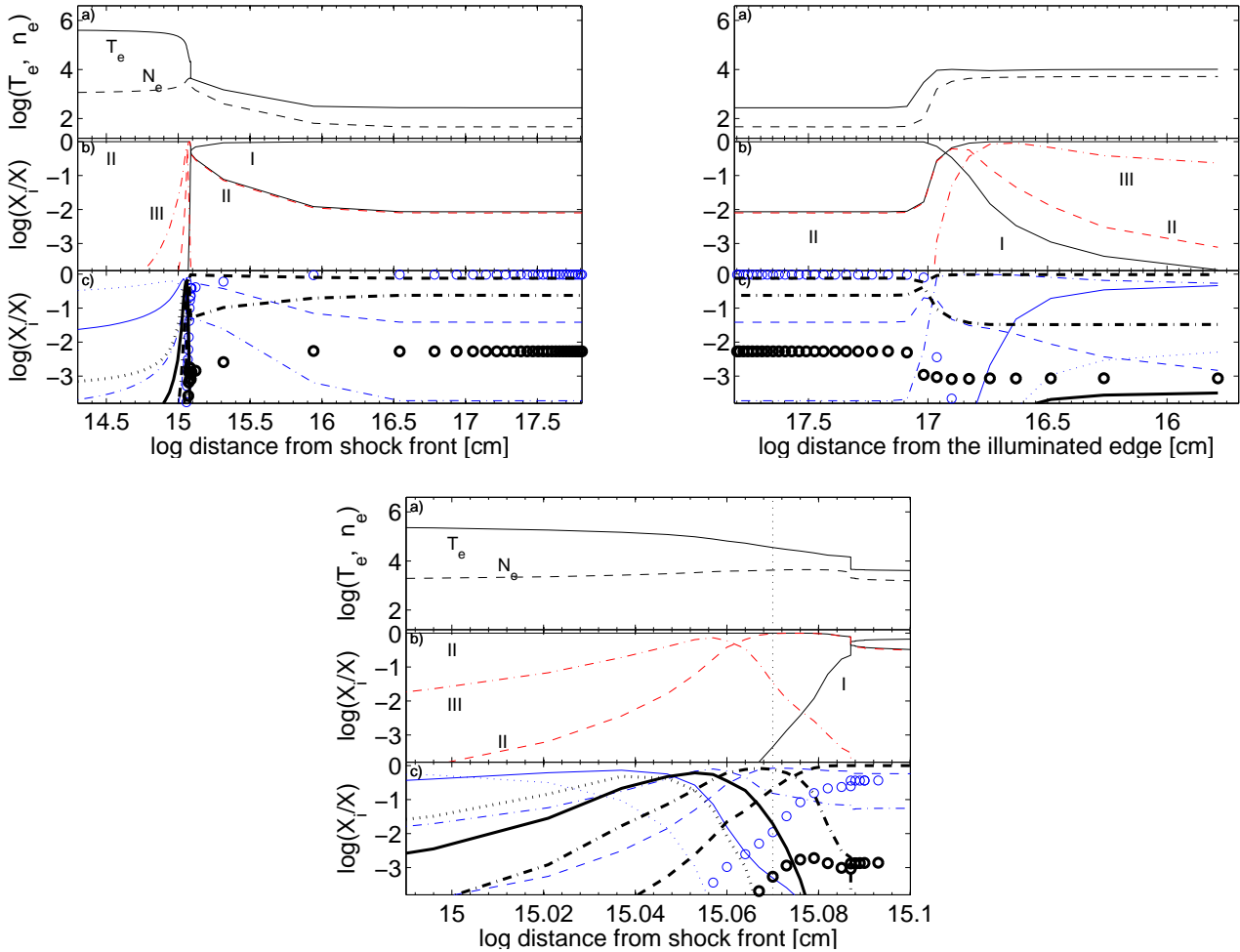


Figure 6. Top diagrams : the RD model mN3 for GRB 031203 (see text). Top panels : the electron temperature and the electron density throughout the emitting cloud. Middle panels : red lines : O^{2+}/O (dot-dashed, III) and O^+/O (dashed, II); black solid lines : H^+/H (II) and H^0/H (I). Bottom panels : blue lines refer to Ne: Ne^{4+}/Ne (dotted), Ne^{3+}/Ne (solid), Ne^{2+}/Ne (dash-dotted), Ne^+/Ne (dashed), Ne^0/Ne (large circles). Black thick lines refer to S : S^{4+}/S (dotted), S^{3+}/S (solid), S^{2+}/S (dash-dotted), S^+/S (dashed), S^0/S (large circles). Bottom diagram : the SD model for GRB 031203. Symbols as in the top diagrams. The vertical black dotted line shows the edge of the emitting cloud

REFERENCES

Allen, C.W. 1976 *Astrophysical Quantities*, London: Athlone (3rd edition)
 Anders, E., Grevesse, N. 1989, *Geochimica et Cosmochimica Acta*, 53, 197
 Asplund, M., Grevesse, N., Sauval, A.J., Scott, P. 2009, *ARAAS*, 47, 481
 Blanchard, P.K. et al 2015 arXiv:1509.07866
 Castro-Tirado, A.J. et al 2001, *A&A*, 370, 398
 Chevalier, R. A. 1982, *ApJ*, 259, L85
 Christensen, L., Vreeswijk, P.M., Sollerman, J. et al 2008, *A&A*, 490, 45
 Contini, M. 2016, *MNRAS*, 460, 3232
 Contini, M. 2015, *MNRAS*, 452, 3795
 Contini, M. 2014, *A&A*, 564, 19
 Contini, M. 2003, *ApJ*, 339, 125
 Contini, M. & Viegas, S.M. 2001a *ApJS*, 132, 211
 Contini, M. & Viegas, S.M. 2001b *ApJS*, 137, 75
 de Ugarte Postigo, A. et al 2014, *A&A*, 563, 62

Drake, S. A. , Ulrich, R. K. 1980 *ApJS*, 42, 351
 Fishman, G.J., Meegan, C.A. 1995 *ARA&A*, 33, 415
 Fynbo, J.P.U. et al 2000, *ApJ*, 542, L89
 Garnavich, P.M. et al 2003, *ApJ*, 582, 924
 Graham, J. F., Fruchter, A. S. 2013, *ApJ*, 774,119
 Graham, J.F. et al 2015 arXiv:1511.00667v
 Grevesse, N. , Sauval, A.J. 1998, *Space Science Reviews*, 85,161
 Hammer, F. et al 2006, *A&A*, 454, 103
 Han, X. H., Hammer, F., Liang, Y. C., Flores, H., Rodrigues, M., Hou, J. L., Wei, J. Y. 2010, *A&A*, 514, 24
 Hjorth, J. et al. 2003, *Nature*, 423, 847
 Hook, I.M., Jorgensen, I., Allington-Smith, J.R., Davies, R.I., Metcalfe, N., Murowinski, R.G., Crampton, D. 2004, *PASP*, 116,425
 Kobulnicky, H.A., Kewley, I.J. 2004, *ApJ*, 617, 240
 Krühler, T. et al 2015 *A&A*, 581, 125
 Levesque, E. M., Berger, E., Kewley, L. J., Bagley, M. M. 2010a, *AJ*, 139, 694

- Levesque, E.M., Kewley, L.J., Berger, E., Jabran Zahid, H. 2010b, *AJ*, 140, 1557
- Michalowski, M.J. et al 2016 arXiv:1609.01742
- Modjaz, M. et al 2008, *AJ*, 135, 1136
- Niino, Y. et al 2016 *Publ. Astron. Soc. Japan*, arXiv:1606.01983
- Osterbrock, D. E. 1974 in *Astrophysics of gaseous nebulae*, San Francisco, W. H. Freeman and Co., 1974. 263 p.
- Paczynski, B. 1998 *AIPC*, 428, 783
- Pagel, B.E.J., Simonson, E.A., Terlevich, R.J., Edmunds, M.G. 1992, *MNRAS*, 255, 325
- Perley, D.A. et al 2016 arXiv:1609.04016
- Piranomonte, S. et al 2015, *MNRAS*, 452, 3293 2005, *NewA*, 11, 103
- Prochaska, J. X. et al. 2004, *ApJ*, 611, 200
- Rigby, J.R., Rieke, G.H. 2004 *ApJ*, 606, 237
- Savaglio, S., Glazerbrook, K., Le Borgue, D. 2009, *ApJ*, 691, 182
- Schulze, S. et al 2014, *A&A*, 566A, 102S
- Seaton, M.J. 1975, *MNRAS*, 170, 475
- Sollerman, J., Östlin, G., Fynbo, J. P. U., Hjorth, J., Fruchter, A., Pedersen, K. 2005, *NewA*, 11, 103
- Stanek, K.Z. et al 2003, *ApJ*, 591, L17
- Thöne, C.C. et al 2008, *ApJ*, 676, 1151
- Thöne, C.C. & de Ugarte Postigo, A. 2014, *GRB Coordinates Network* 16079
- Vergani, S.D. et al 2011 *A&A* 535, A127
- Watson, D. et al 2014, arXiv:1010.1793
- Woosley, S.E. 1993, *ApJ*, 405, 273
- Xu, D. et al 2013, *ApJ*, 776, 98